THE JOURNAL OF BIOLOGICAL CHEMISTRY VOL. 289, NO. 7, pp. 4262–4272, February 14, 2014

Drosophila TRPML Forms PI(3,5)P_2-activated Cation Channels in Both Endolysosomes and Plasma Membrane*

Received for publication, July 30, 2013, and in revised form, December 11, 2013 Published, JBC Papers in Press, December 27, 2013, DOI 10.1074/jbc.M113.506501

Xinghua Feng[‡§], Yu Huang[§¶], Yungang Lu[‡§], Jian Xiong[§¶], Ching-On Wong[§], Pu Yang[§], Jintang Xia[‡], De Chen[‡], Guangwei Du[§¶], Kartik Venkatachalam[§¶‖], Xuefeng Xia[‡1], and Michael X. Zhu[§¶2]**

*From the [‡]Third Affiliated Hospital of Guangzhou Medical University, Guangzhou, China, 510150, the [§]Department of Integrative Biology and Pharmacology, [¶]Graduate Program in Cell and Regulatory Biology, and [‖]Graduate Program in Neuroscience, the University of Texas Health Science Center at Houston, Houston, Texas 77030, and the **Center for Genomic Medicine, Houston Methodist Research Institute, Houston, Texas 77030*

Background: *Drosophila trpml* mutants reproduced many defects associated with mucolipidosis type IV, but the fly TRPML channel remains uncharacterized.
Results: *Drosophila* TRPML is a phosphoinositide-regulated cation channel on endolysosome and plasma membranes.
Conclusion: Fly TRPML largely resembles mammalian TRPML1, but exhibits differences in subcellular localization and pH dependence.
Significance: The data support using *Drosophila* for assessing TRPML1 function.

Transient Receptor Potential mucolipin (TRPML) channels are implicated in endolysosomal trafficking, lysosomal Ca^{2+} and Fe^{2+} release, lysosomal biogenesis, and autophagy. Mutations in human TRPML1 cause the lysosome storage disease, mucolipidosis type IV (MLIV). Unlike vertebrates, which express three TRPML genes, TRPML1–3, the *Drosophila* genome encodes a single *trpml* gene. Although the *trpml*-deficient flies exhibit cellular defects similar to those in mammalian TRPML1 mutants, the biophysical properties of *Drosophila* TRPML channel remained uncharacterized. Here, we show that transgenic expression of human TRPML1 in the neurons of *Drosophila trpml* mutants partially suppressed the pupal lethality phenotype. When expressed in HEK293 cells, *Drosophila* TRPML was localized in both endolysosomes and plasma membrane and was activated by phosphatidylinositol 3,5-bisphosphate (PI(3,5)P_2) applied to the cytoplasmic side in whole lysosomes and inside-out patches excised from plasma membrane. The PI(3,5)P_2-evoked currents were blocked by phosphatidylinositol 4,5-bisphosphate (PI(4,5)P_2), but not other phosphoinositides. Using TRPML A487P, which mimics the varitint-waddler (Va) mutant of mouse TRPML3 with constitutive whole-cell currents, we show that TRPML is biphasically regulated by extracytosolic pH, with an optimal pH about 0.6 pH unit higher than that of human TRPML1. In addition to monovalent cations, TRPML exhibits high permeability to Ca^{2+}, Mn^{2+}, and Fe^{2+}, but not Fe^{3+}. The TRPML currents were inhibited by trivalent cations Fe^{3+}, La^{3+}, and Gd^{3+}. These features resemble more closely to mammalian TRPML1 than TRPML2 and TRPML3, but with some obvious differences. Together, our data support the use of *Drosophila* for assessing functional significance of TRPML1 in cell physiology.

In vertebrates, the mucolipin subfamily of Transient Receptor Potential mucolipin (TRPML)[3] proteins is comprised of three members: TRPML1, TRPML2, and TRPML3 (MCOLN1–3 for gene names) (1). Mutations of TRPML1 in human are linked to a lysosomal storage disease known as mucolipidosis type IV (MLIV), characterized by severe neurodevelopmental delay, progressive vision loss, neurodegeneration, motor defects, and iron-deficiency anemia (2–5). TRPML1 is widely expressed in many cells and it forms non-selective Ca^{2+}-permeable cation channels primarily localized in the late endosomes and lysosomes (1). Cells from MLIV patients display abnormal accumulation of lipids in endolysosomes, enlarged vacuoles (6), and abnormal vesicle trafficking (7). The physiological and cellular defects of MLIV were largely reproduced in mice with the ablation of MCOLN1 gene (8–10), confirming the critical role of TRPML1 in endolysosomal trafficking and its contribution to MLIV.

Compared with TRPML1, less is known about the roles of TRPML2 and TRPML3 in endolysosomal trafficking. The cell type distributions for these two isoforms are also more restricted than that of TRPML1 (1). These two TRPML isoforms have, in general, a broader subcellular distribution than TRPML1 and they are found to be present on the plasma membrane (11, 12). The plasma membrane TRPML2 and TRPML3 channel activities appear to be inhibited by extracellular Na^+, as removing Na^+ from the extracellular solution allowed development of the constitutive TRPML2 and TRPML3 currents (12, 13). In addition, the Na^+ inhibition is further augmented by acidic pH at the extracytosolic side (14, 15). Interestingly, a gain-of-function mutation of TRPML3 (A419P) associated

* This work was supported in part by Grants R01 GM081658 and GM092759 from the National Institutes of Health (to M. X. Z.), postdoctoral fellowships from the Third Affiliated Hospital of Guangzhou Medical University (to X. F. and Y. L.), and the National Natural Science Foundation of China (No.81270868, to X. X.).

[1] To whom correspondence may be addressed: The Third Affiliated Hospital of Guangzhou Medical University, Guangzhou, China, 510150. E-mail: xuefengx@gmail.com.

[2] To whom correspondence may be addressed: Department of Integrative Biology and Pharmacology, The University of Texas Health Science Center at Houston, MSB 4.128, 6431 Fannin St., Houston, Texas 77030. Tel.: 713-500-7505; Fax: 713-500-7444; E-mail: michael.x.zhu@uth.tmc.edu.

[3] The abbreviations used are: TRPML, transient receptor potential mucolipin; MLIV, mucolipidosis type IV; PEI, polyethylenimine.

with the varitint-waddler (Va) phenotype lacks the Na^+ inhibition and shows constitutive inwardly rectifying cation currents on the plasma membrane (13, 16–18). The Va mice show defects in hearing and pigmentation, implicating a key function of TRPML3 in hair cells and melanocytes (19). Substitutions of the equivalent position, as well as a number of nearby amino acids, by proline in TRPML1 or TRPML2 also resulted in constitutive channel activity on the plasma membrane (16, 17, 20). These have allowed convenient characterizations of biophysical properties of these channels (21).

Common to all mammalian TRPML channels is their activation on the cytoplasmic side by phosphatidylinositol 3,5-bisphosphate ($PI(3,5)P_2$), a phosphoinositide enriched in intracellular membranes (22). At least for TRPML1, this effect appears to be antagonized by phosphatidylinositol 4,5-bisphosphate ($PI(4,5)P_2$) (23), the PIP_2 species enriched in the plasma membrane. Thus, it may be assumed that selective bindings between $PI(3,5)P_2$ and $PI(4,5)P_2$ determine the function of TRPML channels. While the high $PI(4,5)P_2$ content inhibits the TRPML channels located on the plasma membrane, the high $PI(3,5)P_2$ levels in intracellular membranes support the activation of TRPML channels in endolysosomes.

Different from vertebrates, *Drosophila melanogaster* and *Caenorhabditis elegans* express only one *trpml* gene. In *C. elegans*, the deletion of the MCOLN ortholog gene, *cup-5*, leads to the accumulation of enlarged vacuoles, excess apoptotic cells, and embryonic lethality (24, 25). In *Drosophila*, disruption of the only *trpml* gene resulted in similar, but more severe, defects as compared with human MLIV, including defective autophagy due to diminished fusion of late-endosomes and amphisomes with lysosomes, impaired synaptic transmission, accumulation of apoptotic cells, oxidative stress, lipofuscin accumulation, mitochondrial dysfunction, motor defects, and massive neurodegeneration (1, 26–28). The more severe abnormality of the *Drosophila* TRPML knock-out than the mammalian TRPML1 knock-out/mutations suggests that the insect channel may also carry out functions that are uniquely performed by mammalian TRPML2 and/or TRPML3, raising the possibility that the insect TRPML channel may collectively possess properties of all three mammalian TRPML channels. To date, however, little is known about the channel function of *Drosophila* TRPML channel and how it is regulated.

Here, we show that transgenic expression of human TRPML1 in neurons of the TRPML-null flies (referred to as $trpml^1$ (26)) partially rescued the pupal lethality phenotype, indicating some but not complete functional resemblance between the insect TRPML and mammalian TRPML1. To provide functional correlates between these channels, we examined the channel function of *Drosophila* TRPML heterologously expressed in HEK293 cells. We show that TRPML is expressed and functional on both endolysosomes and plasma membrane of HEK293 cells. Similar to its mammalian counterparts, it is activated by $PI(3,5)P_2$, and inhibited by $PI(4,5)P_2$. However, its sensitivity to other phosphoinositides is not identical to that of mouse TRPML1. The "Va" mutant of *Drosophila* TRPML is constitutively active on the plasma membrane and is permeable to K^+, Na^+, Cs^+, Ca^{2+}, Mn^{2+}, and Fe^{2+}, but blocked by trivalent cations, Fe^{3+} and La^{3+} and Gd^{3+}. In addition, the channel displays a bell-shaped dependence on extracytosolic pH, which is significantly left shifted as compared with that of human TRPML1.

EXPERIMENTAL PROCEDURES

Plasmids and Compounds—The construct for C-terminal YFP-tagged *Drosophila* TRPML (26) was used to create the TRPML-EGFP plasmid transferring the coding sequence of TRPML to the pEGFP-N1 vector (Clontech). The Lamp1-mCherry plasmid was generated from Lamp1-EGFP (gift from Dr. Paul Luzio, Cambridge University) by replacing the coding sequence of EGFP with that of mCherry. Human $TRPML1^{Va}$-EGFP was a gift from Dr. Haoxing Xu (University of Michigan). $TRPML^{Va}$-EGFP was created by substituting the codon for Ala-487 of TRPML-EGFP by that for a proline using the QuikChange Site-directed Mutagenesis kit (Stratagene). The final sequence was verified by DNA sequencing.

All phosphoinositides (Di-C8 forms, unless indicated otherwise) were purchased from Cayman Chemical Co. Other chemicals were obtained from Fisher Scientific Co or Sigma-Aldrich unless indicated otherwise. Stock solutions of diC16 phospholipids were made in water (0.5 mM) by sonication for 30 min on ice and then aliquots stored at −80 °C. On the day of the experiments, a new aliquot was thawed and diluted in the bath solution for inside-out recordings (see later under "Electrophysiology") and sonicated for 10–30 min. This procedure followed that described previously for $PI(4,5)P_2$ (29), allowing the formation of mostly small micelles for channel activation in the patched membrane.

Transgenic Flies and Pupal Lethality Analysis—The cDNA for C-terminal hemagglutinin (HA)-tagged human TRPML1 (hTRPML1::HA) was subcloned into the pUAST vector and transgenic flies were generated by Rainbow Transgenic Flies Inc. To verify transgene expression in *Drosophila* cells, the flies were crossed with fly line *cg-GAL4* (Bloomington line 7011) for expression in fat-bodies/hemocytes and the presence of hTRPML1::HA in larval fat-bodies was detected by immunohistochemistry as described (27). Briefly, fat-bodies were dissected from 3rd instar wandering larvae and incubated in phosphate-buffered saline (PBS) containing LysoTracker Red DND-99 (1:500) (Invitrogen) at room temperature for 30 min. The samples were then washed two times with PBS, and fixed in 4% paraformaldehyde in PBS for 30 min. Samples were then washed three times with PBS plus 0.1% Triton X-100 before incubating with rabbit anti-HA primary antibodies (Cell Signaling) at 4 °C overnight. The tissues were then washed and probed with fluorophore-conjugated secondary antibodies (Alexa Fluor 488 goat anti-rabbit) (Invitrogen) at room temperature for 1.5 h. Samples were mounted on glass slide with Vectashield Mounting Media containing DAPI (Vector Labs). Images were taken using a Nikon A1 confocal microscope system.

For pupal lethality analysis, hTRPML1::HA was expressed in the $trpml^1$ neurons using a pan-neuronal *GAL4* driver (*elav-GAL4*) as described (26). The numbers of eclosed pupal cases and uneclosed, or partially eclosed, pupae after metamorphosis were counted to determine pupal lethality.

Cell Culture and Transfection—HEK293 cells were cultured as previously described (30). Transfections were performed in

wells of a 96-well plate using polyethylenimine (PEI) (31, 32). Briefly, cells were grown overnight in wells of a 12-well plate to 40–50% confluence. The desired plasmid (0.5 μg) was diluted in 50 μl normal saline (150 mM NaCl, sterile) and then mixed with 4 μl of deacylated PEI (25 mM) by vortexing. After incubation at the room temperature for 10 min, the DNA/PEI mixture was added dropwise to the cultured cells while the plate was gently rocked throughout the process to allow even distribution of the DNA/PEI complex. The plate was then returned to the culture incubator. The cells were reseeded 16–20 h later on poly-ornithine coated glass coverslips and used within 4–24 h for fluorescence imaging or electrophysiological studies.

Fluorescence Imaging—Cells co-transfected with TRPML-EGFP and Lamp1-mCherry grown on glass coverslips were fixed by 4% paraformaldehyde in PBS for 20 min at room temperature and rinsed in PBS. The coverslip was mounted on a glass slide using fluorogel (with Tris buffer) mounting media (Electron Microscopy Sciences). Fluorescence images were taken using a Nikon eclipse Ti laser scanning confocal microscope system. To document the enlarged endolysosomal vacuoles, cells transiently transfected with TRPML-EGFP grown on glass coverslips were treated overnight with vacuolin-1 (1 μM). DIC and epifluorescence images were taken using a 63× water-immersed lens from an upright Olympus BX51WI fluorescence microscope.

Electrophysiology—For whole-cell recordings, the pipette solution contained (in mM): 135 Cs-methanesulfonate, 10 CsCl, 1 $MgCl_2$, 1 EGTA, 4 HEPES (pH 7.2 by CsOH). Recording pipettes were pulled from standard wall borosilicate tubing with filament (Sutter Instrument) to 2–3 MΩ when filled with the pipette solution and placed in the bath. The normal Tyrode's bath solution contained (in mM): 135 NaCl, 5.6 KCl, 2.6 $CaCl_2$, 1 $MgCl_2$, 10 glucose, and 10 HEPES (pH 7.4 by NaOH). The low pH bath solution contained (in mM): 135 NaCl, 5.6 KCl, 2.6 $CaCl_2$, 1 $MgCl_2$, 10 glucose, 10 HEPES, and 10 2-morpholinoethanesulfonic acid (MES), (pH 4.6 or other desired pH values by HCl or NaOH). The *N*-methyl-D-glucamine (NMDG) solution contained (in mM): 140 NMDG, 10 glucose, 10 HEPES (pH 7.4 by HCl). The low sodium bath solution (LSS) contained (in mM): 150 KCl, 2 NaCl, 0.25 $CaCl_2$, 10 glucose, 10 HEPES (pH 7.4 by KOH). For ion selectivity experiments, the isotonic extracellular solution contained (in mM): 150 NaCl, 150 KCl, 150 CsCl, 100 $CaCl_2$, or 100 $MnCl_2$, supplemented with 10 HEPES and 10 MES (pH 4.6 by HCl). For experiments testing permeability of Fe^{2+} and Fe^{3+}, the extracellular Fe^{2+} or Fe^{3+} solution contained (in mM) 50 $FeCl_2$ or 35 $FeCl_3$, supplemented with 10 HEPES and 10 MES and the required amount of NMDG to reach an osmolarity of 300 mOsm (pH 4.6 by HCl). Ascorbic acid (50 μM) was included in the Fe^{2+} solution to prevent oxidation.

For whole lysosome patch clamp recordings, cells transfected with TRPML-EGFP were treated with vacuolin-1 (1 μM) overnight and then placed in the recording chamber mounted on an Olympus IX71-inverted fluorescence microscope. A sharp glass pipette mounted to a micromanipulator was used to slice through a selected EGFP-positive cell that contained enlarged green fluorescence vacuoles (see Fig. 2*B*). One of the vacuoles released from the cell was then picked for whole lysosome recording using a patch electrode filled with the low pH bath solution (pH 4.6) described above. For both whole lysosome and inside-out recordings, the bath solution contained (in mM): 140 K-gluconate, 4 NaCl, 2 $MgCl_2$, 0.39 $CaCl_2$, 1 EGTA, 10 HEPES (pH 7.2 by KOH). The pipette for inside-out recordings contained the normal Tyrode's solution. The pipette resistance was 2–3 MΩ for inside-out patches and 4–5 MΩ for whole-lysosome recordings. The capacitance of the whole lysosomes used for recording was around 1 pF.

Drugs (phosphoinositides and trivalent cations) were diluted to the final desired concentrations in the appropriate solutions and were applied via a gravity-driven perfusion system with the open end placed at about 50 μm from the sample being recorded. The solution exchange was complete within a few seconds.

Data were collected by an EPC9 or EPC10 amplifier using PatchMaster (HEKA electronics Inc., Germany). Cells, patches, or enlarged endolysosomes, were held at 0 mV. Currents were elicited by voltage ramps from −100 to +100 mV in 200 ms and repeated every second. For voltage steps in Fig. 3*C*, 1 s steps from −100 to 90 mV in 10-mV increments and with 2-s intervals were used; for voltage steps in Fig. 5*D*, 400 ms steps from −80 mV to +80 mV in 10-mV increments and with 1-s intervals were used. Signals were digitized at 5 kHz and filtered at 2 kHz. All experiments were conducted at the room temperature (22–23 °C).

Data Analysis—All data were analyzed and plotted using Origin 7.5 (OriginLab, Northampton, MA). Permeability ratios for monovalent cations were determined using the formula: $P_X/P_K = \mathrm{Exp}\,(\Delta E_{rev}F/RT)$, where P_X and P_K are permeabilities of the cation X and K^+, respectively, ΔE_{rev} is the difference between the reversal potential with cation X and that with K^+. F, R, and T are Faraday constant, gas constant, and absolute temperature, respectively. Permeability ratios for divalent cations were calculated using the formula: $P_X/P_{Na} = (37.5/[X]_o)\,\mathrm{Exp}(\Delta E_{rev}F/RT)\times(\mathrm{Exp}(\Delta E_{rev}F/RT)+1)$, where $[X]_o$ represents concentration of the divalent cation in the bath solution and other symbols are the same as defined above. Summary data are presented as the mean ± S.E. Statistical comparisons were made using Student's *t* test. A p value of < 0.05 was considered statistically significant.

RESULTS

Partial Rescue of Pupal Lethality Exhibited by Drosophila trpml-null Mutants Following Neuronal Expression of Human TRPML1—To gain insights on functional correlation between insect TRPML and mammalian TRPML1, we created a transgenic line expressing human TRPML1 in *Drosophila* using the PhiC31 integration system (33). To help confirm the expression in *Drosophila* cells, an HA tag was added to the C terminus of human TRPML1 (*UAS-hTRPML1::HA*), and the transgene was first introduced into fat bodies of wild type flies using *cg-GAL4* because this cell type is enriched in endolysosomes and known to express TRPML (27). Immunostaining using an anti-HA antibody revealed strong fluorescence signals surrounding intracellular vesicles labeled by LysoTracker only in fat bodies dissected from larvae expressing hTRPML1::HA but not in tissues dissected from control flies (Fig. 1*A*), demonstrating that

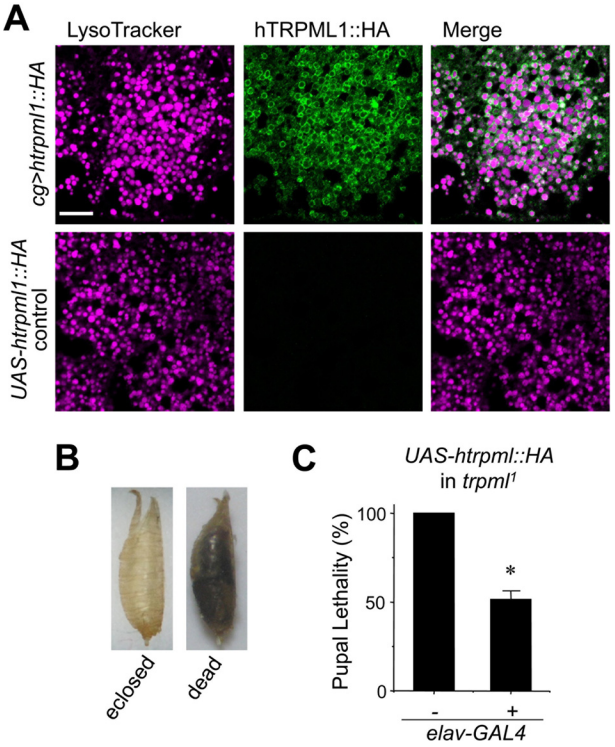

FIGURE 1. **Partial rescue of pupal lethality of *Drosophila trpml*^{1} mutant by neuronal expression of human TRPML1.** *A*, immunohistochemical staining by anti-HA antibody of larval fat-bodies from transgenic flies with *UAS-hTRPML1;HA* expression driven by the *cg-GAL4* driver (*upper panels*) and control flies in which the *UAS-htrpml::HA* transgene was not expressed (*lower panels*). Confocal fluorescence images show LysoTracker Red DND-99 (*violet*) and Alexa Fluor 488 (*green*) stained acidic organelles and hTRPML1::HA, respectively. Scale bar, 10 μm and is the same for all panels. *B*, images of eclosed pupal case and uneclosed (dead) pupa. *C*, pupal lethality of *trpml*^{1} mutant without and with pan-neuronal expression of *UAS-hTRPML1;HA* driven by *elav-GAL4*. $n = 4$ independent crosses. *, $p < 0.001$ *versus trpml*^{1}.

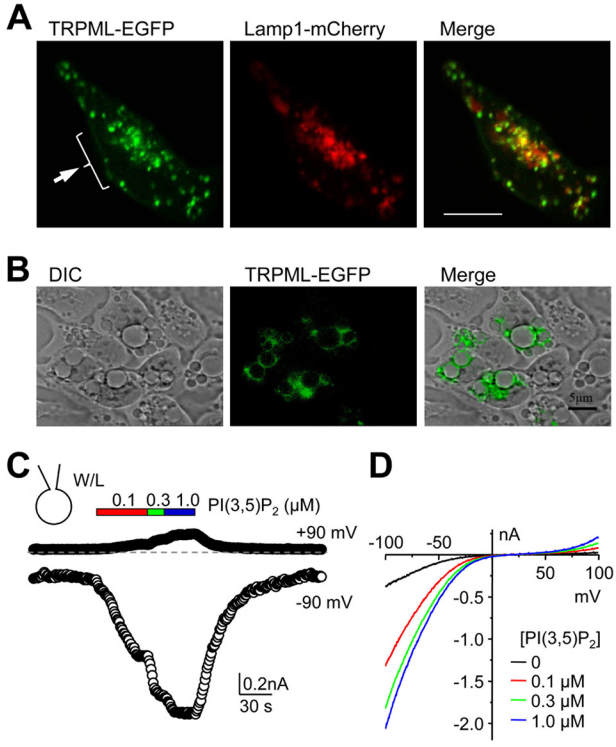

FIGURE 2. **Subcellular distribution of *Drosophila* TRPML expressed in HEK293 cells and PI(3,5)P_2-elicited current in whole-lysosome patches.** *A*, confocal fluorescence images of TRPML-EGFP (*green*) and Lamp1-mCherry (*red*) co-transfected into HEK293 cells. Merged image indicates partial colocalization (*yellow*) between TRPML and Lamp1. Cells were fixed and mounted before sequential images were taken. The *arrow* indicates the presence of TRPML in the perimeter of the cell. Scale bar, 10 μm. *B*, DIC and epifluorescence images of TRPML-EGFP transfected HEK293 cells treated with vacuolin-1 (1 μM, overnight). Merged image shows presence of TRPML-EGFP in the periphery of enlarged vacuoles. Scale bar, 5 μm. *C*, whole-lysosome currents in HEK293 cells that expressed TRPML. Cells were treated with vacuolin-1 overnight and enlarged vacuoles were released by slicing the cell with a sharp glass pipette. The vacuole was held at 0 mV in inside-out mode for whole lysosome and currents elicited by voltage ramps from −100 mV to +100 mV in 200 ms at 1-s intervals. Shown are time courses of currents at −90 and +90 mV for a representative vacuole treated with increasing concentrations of PI(3,5)P_2 (diC8) as indicated. The *dashed line* indicates zero current. *W/L*, whole-lysosome. *D*, current-voltage (I-V) curves obtained by voltage ramps under conditions as indicated for the same vacuole shown in *C*. Similar results were obtained from two other whole-lysosome patches.

hTRPML1::HA can be expressed in insect cells and properly localized to acidic organelles. The *Drosophila trpml*^{1} mutants exhibit reduced viability during the pupal phase of metamorphosis, and this pupal lethality is fully rescued by pan-neuronal expression of *UAS-trpml* (26). To examine whether hTRPML1 could mimic the function of TRPML, we directed *UAS-hTRPML1::HA* into all neurons of *trpml*^{1} using *elav-GAL4*. While the *trpml*^{1} mutant displayed 100% pupal lethality, the transgenic flies had nearly even distributions of eclosed and dead pupae (Fig. 1, *B* and *C*). Therefore, the human channel appeared to be able to partially (~50%) rescue the functional defect of TRPML null mutation in *Drosophila*. These results indicate similarity but also incomplete overlap between the function of these two channels. It was thus important to perform a detailed functional characterization of *Drosophila* TRPML and compare it with that of hTRPML1.

Functional Expression of Drosophila TRPML in Endolysosomes and Plasma Membrane of HEK293 Cells—To study the channel function of TRPML, we expressed the C-terminal EGFP-tagged TRPML in HEK293 cells. This system was chosen because it has been most commonly used for functional studies of mammalian TRPML channels (12–23), providing basis for direct comparison between these channels. As demonstrated previously (26), the expressed EGFP fusion protein was mostly found in intracellular vesicles positively labeled by the late-endosomal/lysosomal membrane marker, Lamp1, indicating late-endosomal/lysosomal expression (Fig. 2*A*). Previous studies have measured ionic currents of expressed mammalian TRPML channels using the whole lysosome patch clamp technique after enlarging endolysosomes by the treatment of vacuolin-1 (21, 22). Consistent with the lysosomal localization, inwardly rectifying currents were detected in vacuolin-1 enlarged vacuoles (Fig. 2*B*) released from TRPML-EGFP transfected HEK293 cells by whole lysosome patch clamp recording under basal non-stimulated conditions and the currents were drastically increased by bath application (to the cytoplasmic side) of diC8 PI(3,5)P_2 in a concentration-dependent manner (0.1–1 μM) (Fig. 2, *C* and *D*). The currents reversed at near zero mV and at positive potentials the currents were nearly undetectable until at voltages higher than +80 mV (Fig. 2*D*). These data demonstrate that like mammalian TRPML1, *Drosophila* TRPML forms PI(3,5)P_2-sensitive channels on endolysosomes.

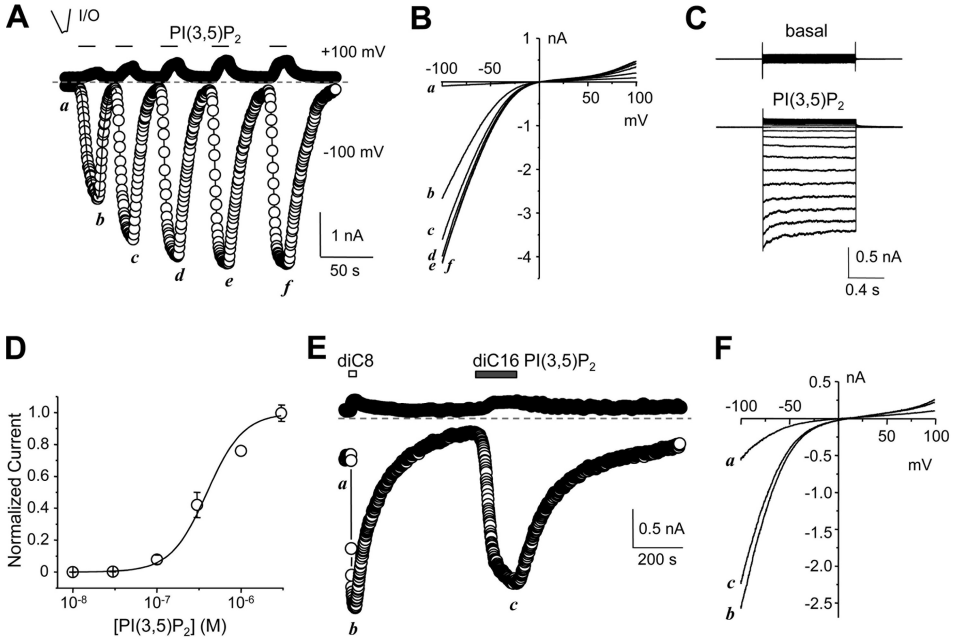

FIGURE 3. **PI(3,5)P_2-evoked current in inside-out patches excised from plasma membrane of HEK293 cells expressing *Drosophila* TRPML.** *A*, representative time courses of currents at −100 mV and +100 mV recorded using voltage ramps from an inside-out (I/O) patch excised from a TRPML-transfected cell. diC8 PI(3,5)P_2 (1 μM) was bath applied multiple times as indicated to the cytoplasmic side. Note the time-dependent run-up of the PI(3,5)P_2-elicited currents. *B*, I-V curves obtained by voltage ramps at the indicated time points in *A*. *C*, representative current traces for the same patch as shown in *A* elicited by voltage steps (−100 to +90 mV, with 10 mV increments, a step duration of 1 s and an interval of 2 s between consecutive steps) from the holding potential of 0 mV in the absence (*upper*) and presence (*lower*) of 1 μM diC8 PI(3,5)P_2. *D*, concentration dependence of diC8 PI(3,5)P_2-evoked currents from inside-out patches. Currents were measured using the similar protocol as in *A*, with varying concentrations of diC8 PI(3,5)P_2 after the currents elicited by 1 μM diC8 PI(3,5)P_2 had stabilized. Current amplitudes at −100 mV were normalized to that elicited by 1 μM diC8 PI(3,5)P_2. Data points (means ± S.E., $n = 7$) were fitted with the Hill equation, which yielded an EC_{50} of 0.39 ± 0.07 μM. *E*, similar to *A*, but with consecutive application of diC8 PI(3,5)P_2 and diC16 PI(3,5)P_2 (both at 3 μM) as indicated. Note the slow rise of current elicited by diC16 PI(3,5)P_2. *F*, I-V curves obtained by voltage ramps at the indicated time points in *E*.

In addition to the intracellular localization, obvious EGFP signal was also observed in the peripheral regions of the TRPML-EGFP transfected cells (Fig. 2*A*, *arrow*), suggesting that a fraction of the expressed proteins might be on the plasma membrane. This differs from mammalian TRPML1, which is almost extensively localized to endolysosomes (21, 22), but resembles TRPML2 and TRPML3, which are present on plasma membrane (11–13). To examine if functional channels were formed on the plasma membrane by TRPML-EGFP, we recorded ionic currents by voltage clamp recordings. No obvious current was detected from transfected cells under the whole-cell configuration with the cells placed in the normal Tyrode's bath solution (data not shown). We also tried two methods that have been previously used to help reveal whole-cell currents for mammalian TRPML2 and TRPML3: (a) using a low sodium bath solution (LSS) (12); and (b) prewashing the cells with an *N*-methyl-D-glucamine (NMDG) solution (NMDG was the only cation) and then adding back the normal Tyrode's bath (13, 14). However, neither method elicited any obvious current (data not shown).

We reasoned that the channel might be dependent on PI(3,5)P_2 for activation and inhibited by the high PI(4,5)P_2 content on the plasma membrane, just like mammalian TRPML1 (22, 23). To test this, we employed the inside-out (I/O) configuration, which allows application of drugs from the cytoplasmic side of the membrane. Micropatches were excised from the transfected cells and placed in the bath solution that mimicked the cytosolic ionic environment. Application of PI(3,5)P_2 (1 μM) in the bath (cytoplasmic side) elicited robust inwardly rectifying currents in approximately one-half of the excised I/O patches (Fig. 3*A*), which were not observed in non-transfected HEK293 cells. Similar to the results from the whole lysosome recordings, the currents reversed at near zero mV and the outward currents at positive potentials were very small (Fig. 3*B*). The PI(3,5)P_2-induced currents also displayed a strong inward rectification in response to voltage steps, showing slight time-dependent inactivation only at voltages lower than −60 mV (Fig. 3*C*). Furthermore, in the continued presence of PI(3,5)P_2, the currents elicited by the voltage ramps also did not show obvious inactivation (data not shown).

Notably, the PI(3,5)P_2-induced current increased gradually with repeated PI(3,5)P_2 applications, and reached a steady-state level after 3–4 stimulations (Fig. 3*A*). Therefore, the subsequent experiments were conducted after the currents had become stable with four repeated applications of PI(3,5)P_2 (1 μM). After that, the concentration dependence on PI(3,5)P_2 was tested and yielded an EC_{50} of 0.39 ± 0.07 μM ($n = 7$) for TRPML (Fig. 3*D*).

The above experiments used diC8 PI(3,5)P_2, which contains shorter acyl chains than the physiological phospholipids. To test if the full-length PI(3,5)P_2 could also activate TRPML, we applied diC16 PI(3,5)P_2 to the I/O patches after the response to 1 μM diC8 PI(3,5)P_2 had become stable. At 1 μM, diC16 PI(3,5)P_2 did not consistently elicit a response, but at 3 and 10 μM, it induced TRPML current with a similar current-voltage (I-V) relationship as that evoked by diC8 PI(3,5)P_2 (Fig. 3, *E* and *F*). Noticeably, the current developed more slowly in diC16 than in diC8 PI(3,5)P_2. The time to reach half-maximal ampli-

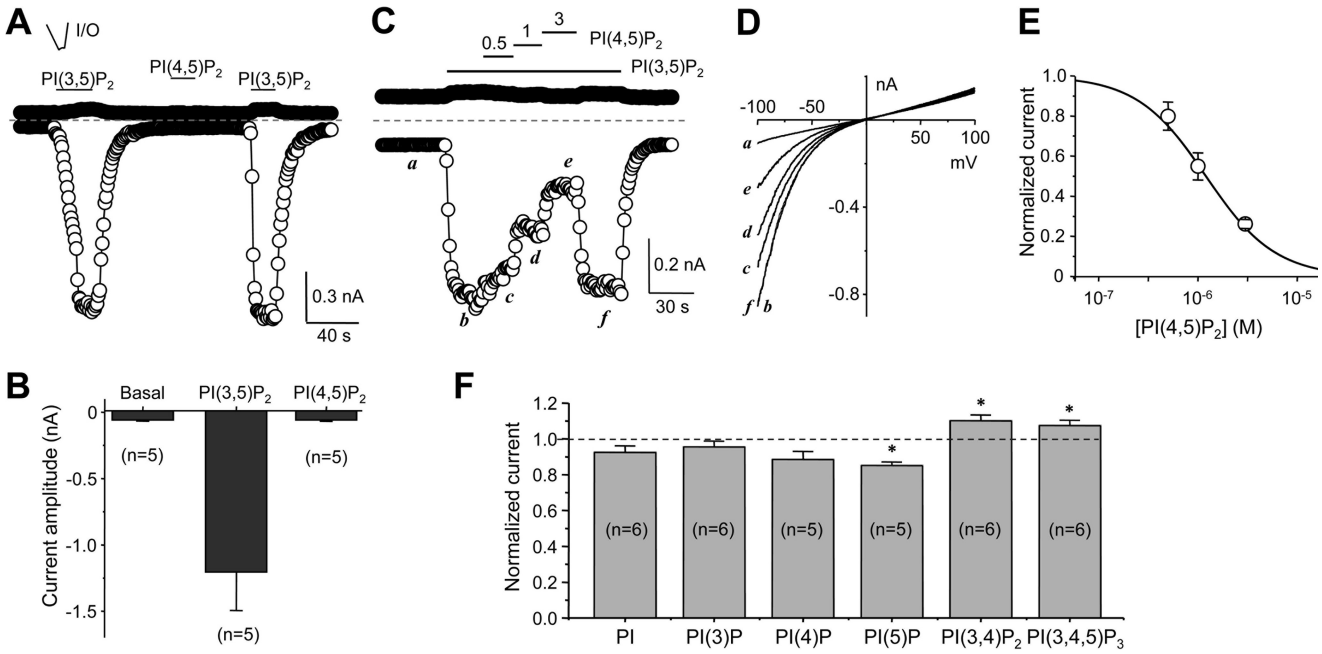

FIGURE 4. **Inhibition of TRPML by PI(4,5)P_2.** *A*, representative time courses of currents at −100 mV and +100 mV recorded using voltage ramps from an inside-out (I/O) patch excised from a TRPML-transfected cell. PI(3,5)P_2 or PI(4,5)P_2 (both diC8 and at 1 μM) was bath applied to the cytoplasmic side as indicated. *B*, summary data (means ± S.E.) for currents at −100 mV under basal (no phosphoinositide applied), PI(3,5)P_2- and PI(4,5)P_2-treated conditions. *C*, inhibition of PI(3,5)P_2-elicited currents by PI(4,5)P_2. Similar to *A*, but with different concentrations of PI(4,5)P_2 applied while the patch was exposed to 0.3 μM PI(3,5)P_2, demonstrating concentration-dependent inhibition of the PI(3,5)P_2-elicited currents by PI(4,5)P_2. *D*, I-V curves obtained by voltage ramps at the indicated time points in *C*. *E*, summary ($n = 4$) of currents at −100 mV normalized to that activated by 0.3 μM PI(3,5)P_2. Data points were fitted with the a dose response equation: $y = 1/(1 + 10^{\wedge}(\text{Log}(IC_{50})\text{-}x)^n)$. *F*, summary (means ± S.E.) of the effects of indicated phosphoinositides on PI(3,5)P_2-evoked TRPML current in inside-out patches. Phosphoinositides were used at 3 μM and PI(3,5)P_2 was at 0.3 μM. Current amplitudes at −100 mV were normalized to that evoked by PI(3,5)P_2 alone. *, $p < 0.01$ *versus* PI(3,5)P_2 alone.

tude ($T_{1/2}$) was 2.4 ± 0.5 s for 1 μM diC8 and 28.8 ± 2.7 s for 3 μM diC16 PI(3,5)P_2 ($n = 6$ for each, $p < 0.01$, paired *t* test). In addition, the current elicited by 10 μM diC16 PI(3,5)P_2 was difficult to wash out (data not shown). The peak current elicited by 3 μM diC16 PI(3,5)P_2 was 83.2 ± 9.3% of that evoked by 3 μM diC8 PI(3,5)P_2 ($n = 7$). Thus, TRPML was also activated by the full-length PI(3,5)P_2 applied from the cytosolic side of I/O patches. The long acyl chain appeared to slow down TRPML activation by the phospholipid in I/O patches. The slower activation kinetics has also been reported for currents of plasma membrane localized K^+ channels activated by PI(4,5)P_2 of longer acyl chains than shorter ones (29, 34), presumably because of micelle formation. In subsequent experiments, we only used the diC8 forms of phosphoinositides.

Inhibition of TRPML by PI(4,5)P_2—The run-up of PI(3,5)P_2-induced currents in I/O patches is consistent with the observation that mammalian TRPML1 is inhibited by PI(4,5)P_2, which is enriched on the plasma membrane and slowly washed out under the I/O patch configuration in the absence of ATP (23). Therefore, we tested whether PI(4,5)P_2 could inhibit the TRPML currents. Although very similar in structure, PI(4,5)P_2 (1 μM) did not evoke the TRPML current from I/O patches like PI(3,5)P_2 did when applied alone (Fig. 4, *A* and *B*). Instead, it inhibited the currents activated by PI(3,5)P_2 in a concentration-dependent manner (Fig. 4, *C--E*). At 3 μM PI(4,5)P_2, which is lower than the resting plasma membrane PI(4,5)P_2 concentration of 4–10 μM (23), the current evoked by PI(3,5)P_2 (0.3 μM) at −100 mV was inhibited by about 75% (73.8 ± 1.1%, $n = 4$). The IC_{50} for PI(4,5)P_2 inhibition was estimated to be 1.21 μM ($n = 4$).

To gain information about selectivity of TRPML among different phosphoinositides, we tested the effect of PI, PI(3)P, PI(4)P, PI(5)P, PI(3,4)P_2, and PI(3,4,5)P_3 (all diC8) on PI(3,5)P_2-induced current in the I/O patches excised from cells that expressed TRPML-EGFP. At 1 μM, none of the phosphoinositides significantly changed the basal current in the I/O patches, in which robust currents were elicited by PI(3,5)P_2 (data not shown), suggesting that activation of TRPML is specifically dependent on PI(3,5)P_2. We then used 10-fold excess of the phosphoinositide concentration (3 μM) to test the effect on current elicited by PI(3,5)P_2 (0.3 μM). Only PI(5)P caused significant, but small (15 ± 2%), inhibition, while PI(3,4)P_2 and PI(3,4,5)P_3 resulted in small (~10%), but significant, increase of the current (Fig. 4*F*). This profile is different from that of mouse TRPML1, for which PI(3,4)P_2 and PI(3,4,5)P_3 were equally potent as PI(4,5)P_2 at inhibiting the current evoked by PI(3,5)P_2 (23).

pH Dependence of TRPML—The A419P mutation of mouse TRPML3 (*Va* mutant) led to constitutive channel activation and accumulation of the mutant channels on the plasma membrane. Equivalent mutations, but with V→P substitution for mammalian TRPML1 and A→P for TRPML2 also caused the similar effect (16, 17). Based on the alignment with mammalian TRPMLs (Fig. 5*A*), we mutated A487 of TRPML to a proline (A487P) to create $TRPML^{Va}$. As expected, expression of $TRPML^{Va}$ in HEK293 cells led to constitutive inwardly rectify-

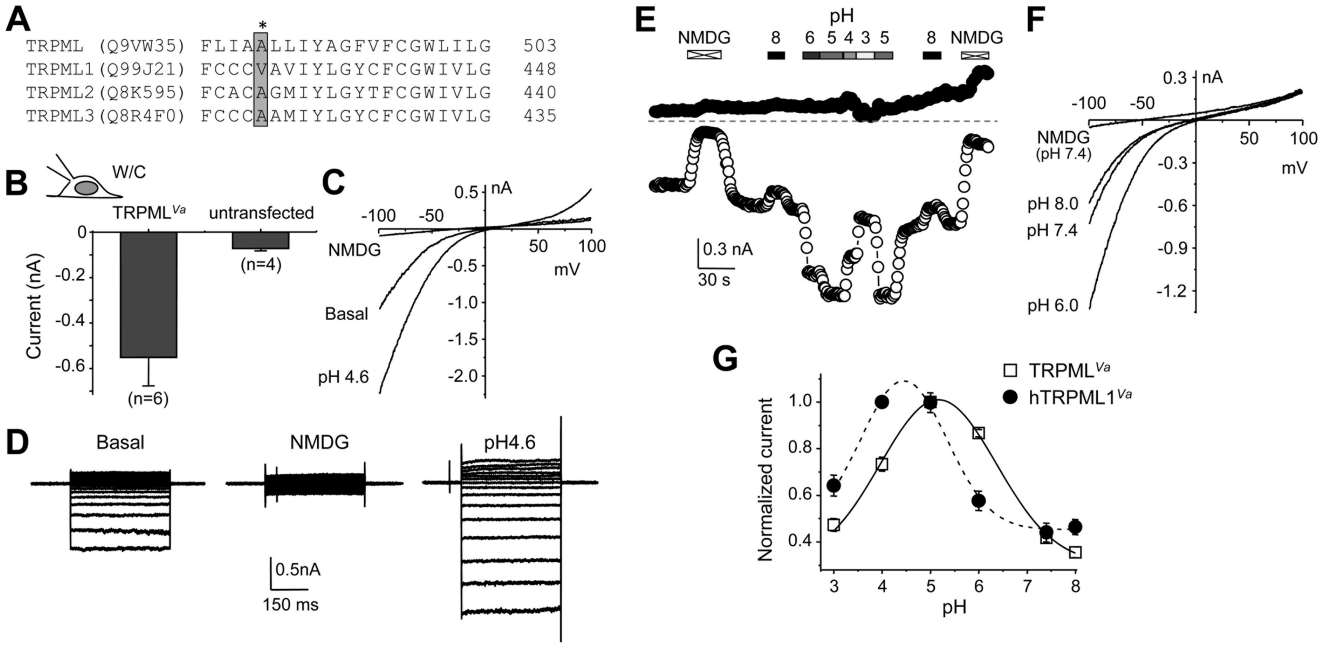

FIGURE 5. **Whole-cell currents of *Drosophila* TRPML^{Va} expressed in HEK293 cells and its dependence on extracytosolic pH.** *A*, alignment of putative transmembrane segment 5 of *Drosophila* TRPML with that of mouse TRPML1, TRPML2, and TRPML3. Names in *parentheses* are Gene Product ID in UniProtKB database. The amino acids mutated in the Va mutants are *boxed* and shaded in *gray*. The *asterisk* indicates Ala-487 of *Drosophila* TRPML, which was replaced with a proline in TRPML^{Va}. *B*, summary (means ± S.E.) of current amplitudes at −100 mV from whole-cell recordings of basal activity in normal Tyrode's bath solution by voltage ramps in HEK293 cells expressing TRPML^{Va} or untransfected cells. *C*, representative I-V curves obtained by voltage ramps of whole-cell recording of an HEK293 cell expressing TRPML^{Va} in normal Tyrode's bath solution (basal), NMDG bath, and pH 4.6 Tyrode's bath. *W/C*, whole-cell. *D*, representative traces of whole-cell currents elicited by voltage steps (−80 mV to +80 mV, with 10-mV increments and a step duration of 400 ms) from the holding potential of 0 mV in an HEK293 cell expressing TRPML^{Va} in normal Tyrode's (basal, *left*), NMDG (*middle*), and pH 4.6 Tyrode's (*right*) bath solutions. *E*, representative time courses of currents at −100 mV and +100 mV recorded using voltage ramps by whole-cell recording of an HEK293 cell expressing TRPML^{Va}. Constitutive basal currents were seen in normal Tyrode's bath. NMDG and Tyrode's solutions with different pH were applied as indicated through perfusion. *F*, I-V curves obtained by voltage ramps for selected conditions shown in *E*. *G*, summary of pH-dependent modifications of TRPML^{Va} and human TRPML1^{Va} (hTRPML1^{Va}). Currents at −100 mV were normalized to that recorded in pH 5.0 Tyrode's bath. Data points (means ± S.E., $n = 5$ for each) were fitted with Gaussian function.

ing currents readily detectable upon formation of the whole-cell configuration (Fig. 5, *B* and *C*). The inward rectification and reversal potential at near-0 mV were in agreement with the I-V relationship recorded for wild type TRPML from whole-lysosomes and I/O plasma membrane patches. The inward current of TRPML^{Va} was eliminated by substitution of all cations in the Tyrode's bath solution with NMDG (Fig. 5*C*), demonstrating cation selectivity. In response to voltage steps, the constitutive currents showed persistent currents at negative potentials with no obvious inactivation in 400 ms (Fig. 5*D*, *left*). These currents were again eliminated by the NMDG bath solution (Fig. 5*D*, *middle*). Therefore, the TRPML^{Va} mutant displays constitutive activity on the plasma membrane without an obvious change in the biophysical properties. It is thus a suitable construct for further characterizations of TRPML properties when solution exchanges needed to be carried out from the extracellular side (equivalent to lysosome lumen). Similar approaches have been used to study the properties of mammalian TRPML channels (15, 16, 21).

It was previously shown that extracellular acidification (pH 4.6) enhanced the current of mouse TRPML1^{Va} but reduced that of TRPML3^{Va} (16). As a lysosomal channel, TRPML is also exposed to the acidic pH of the endolysosomal lumen. Therefore, it was important to know how its activity was affected by pH changes. Similar to mouse TRPML1^{Va}, lowering extracellular pH from pH 7.4 to pH 4.6 markedly increased the TRPML^{Va} currents by about 2-fold (Fig. 5, *C* and *D*, *right*). To further define the pH dependence of TRPML, we exposed the TRPML^{Va}-expressing cells to a range of extracellular pH values, from pH 3 to 8 (Fig. 5*E*). Interestingly, the pH dependence is bell-shaped, with current peaked in between pH 5 and 6 and declined at either higher or lower pH values (Fig. 5, *E* and *F*). Fitting normalized currents at −100 mV in different extracellular pH solutions with a Gaussian function yielded an optimal pH of 5.17 ± 0.04 for TRPML^{Va}, which is about 0.6 pH unit less acidic than that of human TRPML1^{Va} (4.45 ± 0.07), determined under the same conditions. Therefore, TRPML activity is potentiated by acidic pH commonly found in the lumen of endolysosomes but inhibited by strong acid. Compared with mammalian TRPML1, the pH dependence of TRPML is shifted to milder acidity.

Ion Selectivity of TRPML—Elimination of the inward currents by NMDG suggested that TRPML^{Va} mediated cation currents (Figs. 5, *C* and *D*, and 6, *A* and *B*). To determine the ion selectivity of TRPML^{Va}, we replaced the Tyrode's bath solution with isotonic solutions of different cations in the whole-cell configuration (Fig. 6*A*). The divalent-free (DVF) isotonic KCl solution caused an immediate increase in current amplitudes from that in the Tyrode's solution at all potentials and then quickly reduced to an intermediate level. Switching to a DVF NaCl solution caused a further increase of the current amplitudes, which was strongly reduced by exchanging for a DVF CsCl solution (Fig. 6*A*). The relative currents of K^+ and Cs^+ to

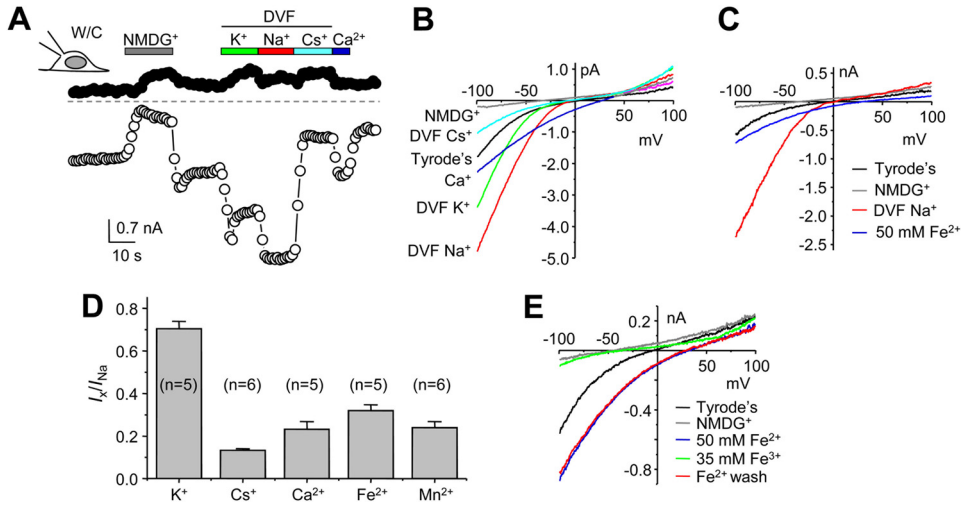

FIGURE 6. **Cation permeability of *Drosophila* TRPML^{Va}.** *A*, representative time courses of currents at −100 mV and +100 mV recorded using voltage ramps by whole-cell recording of an HEK293 cell expressing TRPML^{Va}. Constitutive basal currents were seen in normal Tyrode's bath. Divalent-free (*DVF*) isotonic NMDG, K^+, Na^+, and Cs^+ solutions, as well as an isotonic Ca^{2+} solution, were applied as indicated. *B*, I-V curves obtained by voltage ramps in different extracellular solutions as indicated, for the same cell as in *A*. *C*, I-V curves of whole-cell currents obtained by voltage ramps for another cell exposed to normal Tyrode's, DVF isotonic Na^+ and NMDG, and Fe^{2+} (50 mM) solutions. *D*, summary (means ± S.E.) of current amplitudes at −100 mV in DVF isotonic K^+ and Cs^+, isotonic Ca^{2+} and Mn^{2+}, and 50 mM Fe^{2+} normalized to that in DVF isotonic Na^+. *E*, I-V curves of whole-cell currents obtained by voltage ramps for an HEK293 cell expressing TRPML^{Va} exposed sequentially to normal Tyrode's, NMDG, 50 mM Fe^{2+}, 35 mM Fe^{3+} solutions. The current recovered after washout in 50 mM Fe^{2+}. pH was 4.6 for all solutions except for normal Tyrode's and NMDG solutions, which had pH of 7.4.

that of Na^+ at −100 mV were 0.70 ± 0.4 ($n = 5$) and 0.13 ± 0.01 ($n = 6$), respectively (Fig. 6*D*). The permeability ratios of Na^+/K^+ and Cs^+/K^+ were 1.00 ± 0.06 ($n = 3$) and 1.00 ± 0.02 ($n = 7$), respectively, based the calculation using reversal potential values, suggesting about equal permeability to Na^+, K^+, and Cs^+ for the heterologously expressed TRPML^{Va} channel.

We also tested the permeability to Ca^{2+} and Fe^{2+}, both have been shown to permeate mouse TRPML1^{Va} (16, 21). Switching the extracellular solution to 100 mM $CaCl_2$ or 50 mM $FeCl_2$ markedly reduced the inward currents as compared with that in DVF isotonic NaCl, but the reversal potentials were changed to more positive than zero mV (Fig. 6, *B* and *C*), indicating that TRPML^{Va} had higher permeabilities for Ca^{2+} and Fe^{2+} than monovalent cations. The relative currents of Ca^{2+} and Fe^{2+} to that of Na^+ at −100 mV were 0.23 ± 0.04 ($n = 5$) and 0.32 ± 0.03 ($n = 3$), respectively (Fig. 6*D*). The permeability ratios of Ca^{2+}/Na^+ and Fe^{2+}/Na^+ were 5.5 ± 1.2 ($n = 8$) and 12.0 ± 2.0 ($n = 5$), respectively, based the calculation using reversal potential values. The expressed TRPML^{Va} channel also showed permeability to Mn^{2+}. The relative current of Mn^{2+} to that of Na^+ at −100 mV was 0.24 ± 0.03 ($n = 6$) (Fig. 6*D*) and the permeability ratio of Mn^{2+}/Na^+ was 6.0 ± 1.8 ($n = 5$).

Inhibition of TRPML by Trivalent Cations—In contrast to Fe^{2+}, TRPML^{Va} was impermeable to Fe^{3+}. With the bath solution containing 35 mM $FeCl_3$, nearly no inward current was detectable, but the current recovered completely upon washout by 50 mM $FeCl_2$ (Fig. 6*E*). Not only was Fe^{3+} not able to permeate TRPML^{Va}, but also it inhibited the cation conductance of TRPML^{Va} in a concentration dependent manner (Fig. 7, *A* and *B*). In the pH 4.6 Tyrode's solution, addition of 1 mM $FeCl_3$ inhibited the current at −100 mV by 36.2 ± 1.0% ($n = 3$) and 10 mM $FeCl_3$ inhibited the current by 72.5 ± 2.6% ($n = 3$).

Lanthanides, La^{3+} and Gd^{3+}, have been frequently found to block non-selective cation channels, including many TRP channels (35). Including 1 mM La^{3+} or Gd^{3+} in the pH 7.2 Tyrode's solution blocked the TRPML^{Va} current at −100 mV by 78 ± 2 or 74 ± 3%, respectively (Fig. 7, *C*, *D*, *G*). These levels of inhibition were similar to the inhibition of human TRPML1^{Va} by the lanthanides (Fig. 7*G*). Interestingly, the degree of inhibition by both lanthanides was comprised in acidic extracellular pH and the effect was more pronounced for La^{3+} than Gd^{3+}. At pH 4.6, 1 mM La^{3+} inhibited the TRPML^{Va} current by 35 ± 3%, and 1 mM Gd^{3+} inhibited it by 55 ± 3% (Fig. 7, *E*–*G*). These data suggest that like mammalian TRPML1, TRPML is inhibited by lanthanides and the inhibition is weakened by acidic pH commonly found in the lysosome lumen.

DISCUSSION

Unlike mammals, the fruit fly *Drosophila melanogaster* expresses only one TRPML isoform (26). Nonetheless, ablation of the *Drosophila trpml* gene in flies reproduced many of the cellular defects found in MLIV human patients and in *MCOLN1* knock-out mice (26, 27), suggesting conserved functions in cellular physiology between fly TRPML and mammalian TRPML1. However, the lack of TRPML2 and TRPML3 would suggest that TRPML might also carry functions normally performed by these two TRPML isoforms in mammalian cells, which could help explain some of the more severe cellular abnormalities found in the *Drosophila* mutant than mammalian TRPML1 mutants. Indeed, we found that transgenic expression of human TRPML1 in neurons of *Drosophila trpml*-null mutant partially rescued the pupal lethality phenotype, demonstrating the conserved function between TRPML1 and TRPML. However, unlike the fly TRPML, which completely rescued pupal lethality when expressed using the same pan-neuronal promoter (26), the rescue by the human channel was only about 50%, indicating also significant functional divergence between the two channels. Thus, functional characterization of TRPML is an important step toward better understanding of molecular

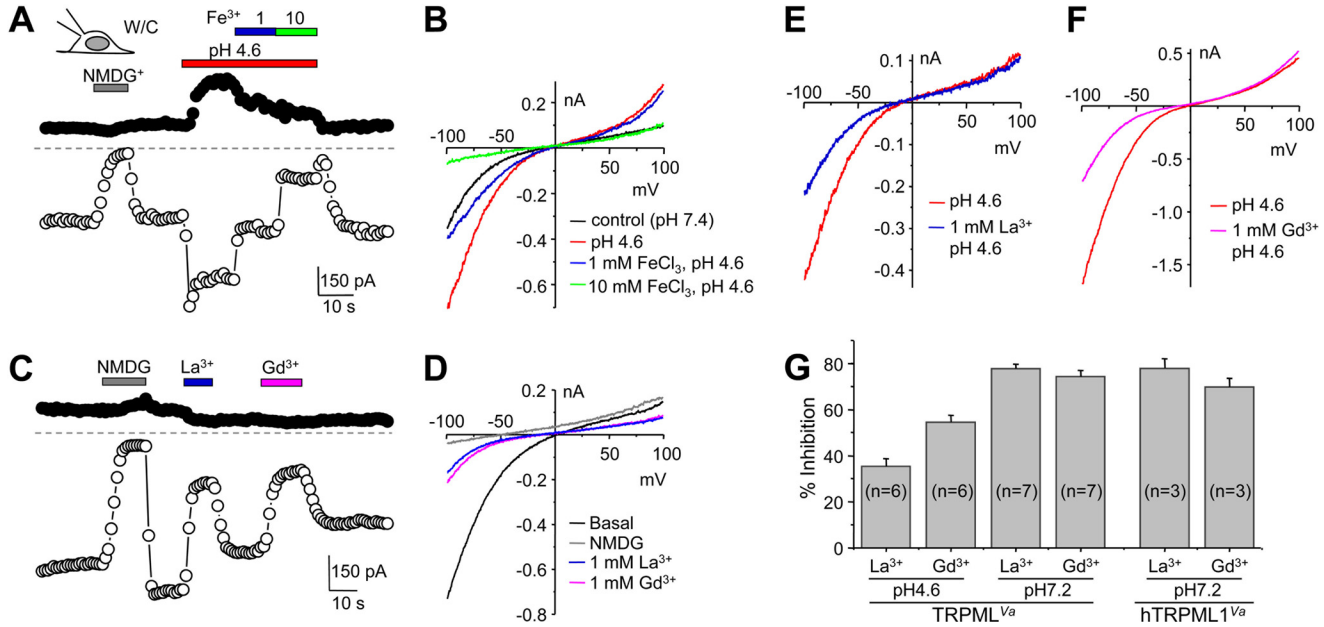

FIGURE 7. **Inhibition of TRPML^{Va} current by trivalent cations.** *A*, representative time courses of currents at −100 mV and +100 mV recorded using voltage ramps by whole-cell recording of an HEK293 cell expressing TRPML^{Va}. The cell was exposed to normal Tyrode's NMDG, pH 4.6 Tyrode's, and pH 4.6 Tyrode's solution containing 1 and 10 mM $FeCl_3$ as indicated, showing concentration dependent inhibition by Fe^{3+}. *B*, I-V curves obtained by voltage ramps under conditions shown in *A*. *C* and *D*, similar to *A* and *B*, but pH 7.2 Tyrode's solution was used, and 1 mM $LaCl_3$ and 1 mM $GdCl_3$ in the pH 7.2 Tyrode's were applied as shown. *E* and *F*, I-V curves obtained by voltage ramps from whole-cell recording of two different TRPML^{Va}-transfected cells exposed to pH 4.6 Tyrode's solution without or with 1 mM $LaCl_3$ (*E*), or $GdCl_3$ (*F*). *G*, summary data (means ± S.E.) for % inhibition by La^{3+} and Gd^{3+} (both at 1 mM) of whole-cell currents at −100 mV in HEK293 cells that expressed either TRPML^{Va} or hTRPML1^{Va}. The extracellular solution had pH either at 4.6 or 7.2 as indicated.

mechanisms of TRPML channel regulation and physiological function.

In the current study, we characterized, for the first time, the channel function of *Drosophila* TRPML. When expressed in HEK293 cells, TRPML is present in both lysosomal compartments and plasma membrane. $PI(3,5)P_2$-sensitive inwardly rectifying currents are detectable in both whole-lysosome recordings from vacuolin 1-enlarged vacuoles and inside-out patches excised from plasma membrane. The $PI(3,5)P_2$-elicited current is inhibited by $PI(4,5)P_2$ but not other commonly found phosphoinositides. Using the equivalent *Va* mutant as that described for mammalian TRPML channels, we demonstrate that TRPML is under bimodal modulation by pH at the extracytosolic side and is permeable to monovalent and divalent cations but blocked by trivalent cations such as Fe^{3+}, La^{3+}, and Gd^{3+}. These features are similar to mammalian TRPML channels. The facts that the expressed *Drosophila* TRPML in HEK293 cells recapitulated subcellular localizations of native TRPML in fly cells and displayed channel function in a manner largely similar to mammalian TRPML1 suggest that the properties described here are most likely intrinsic to TRPML protein itself without a need of auxiliary subunits, at least those from *Drosophila*.

However, there are important differences between the *Drosophila* and mammalian TRPML channels. First of all, TRPML is localized both in the lysosomes and on the plasma membrane. This agrees with the observed subcellular distributions of TRPML protein in *Drosophila* cells, where a shift from plasma membrane to endolysosomal localization was found to be promoted by the initiation of autophagy (27). Different from mammalian TRPML1, which is expressed mainly in endolysosomes and only at a very low level at the plasma membrane (21–23), the *Drosophila* TRPML exhibited significant channel expression on the plasma membrane, as shown by the robust $PI(3,5)P_2$-elicited macroscopic current in excised inside-out patches. Intriguingly, the success rate of obtaining functional patches was about 50%; the patch either had no obvious current, not even single channel current, or exhibited macroscopic current in response to bath application of $PI(3,5)P_2$. This suggests that the plasma membrane TRPML most likely exists in clusters.

The plasma membrane localization of TRPML resembles that of mammalian TRPML2 and TRPML3 (12–14). However, different from these channels, the plasma membrane TRPML channels cannot be activated by exposing cells to a solution that contained no or a low concentration of Na^+. Therefore, the TRPML channel does not appear to have the Na^+ sensitivity exhibited by the wild type TRPML2 and TRPML3 (12). On the other hand, although it has not been directly determined whether mammalian TRPML1 exhibits sensitivity to extracellular Na^+, in whole lysosome patches, the $PI(3,5)P_2$-elicited TRPML1 current was not affected by the luminal Na^+ (22) and in whole-cell recordings, extracellular Na^+ supported inward currents mediated by the surface expressed TRPML1–4A mutant (23, 36). Therefore, TRPML appears to resemble mammalian TRPML1 for lacking sensitivity to Na^+ block. Note that the Na^+ sensitivity of TRPML2 and TRPML3 is lost in the *Va* mutants (13, 15). The *Va* mutations render all mammalian TRPML channels constitutively active. The equivalent mutation in *Drosophila* TRPML, A487P, also displays strong constitutive currents in whole-cell recordings.

Also similar to TRPML1 is the Fe^{2+} permeability of TRPML. Both TRPML1 and TRPML2, have been shown to permeate Fe^{2+} and TRPML1 was suggested to play a critical role in Fe^{2+} release from late endosomes and lysosomes, a function severely

impaired in cells from MLIV patients. However, TRPML3 showed little or no Fe^{2+} permeability (21). We show that TRPML is permeable to Fe^{2+}, with a permeability about 12 times that of Na^+. In addition, TRPML also exhibited excellent permeability to other divalent cations, Ca^{2+} and Mn^{2+}. These properties resemble that of mammalian TRPML1.

In contrast to the permeation to divalent cations, TRPML is impermeable to trivalent iron, Fe^{3+}. Rather, the channel is blocked by Fe^{3+}, as well as lanthanides, La^{3+} and Gd^{3+}. The block is more pronounced in neutral than acidic pH. This property has not been described for mammalian TRPML channels, although the monovalent conductance of TRPML1 has been shown to be inhibited by Fe^{2+} (21).

TRPML exhibits equal permeability to Na^+, K^+, and Cs^+, but is impermeable to the large organic monovalent cation, NMDG. The current amplitude displays an order of $Na^+ > K^+ > Cs^+$ in the absence of divalent cations. The smaller K^+ current than Na^+ current may be partially explained by the fast inactivation upon switching to the DVF K^+ solution (see Fig. 6*A*).

The pH dependence of TRPML is very interesting. For both the fly TRPML and human TRPML1, we show bell-shaped dependence on extracytosolic pH, which is equivalent to the pH in lysosomal lumen. However, the pH dependence curve for the human channel is shifted to more acidic range than that for *Drosophila* TRPML by about 0.6 pH unit. This suggests that optimal activity of TRPML is achieved at less acidic pH than that of mammalian TRPML1. Intriguingly, the lysosomal pH of fly cells is around 5.1 (37), which is more neutral than that of mammalian cells (38, 39). Therefore, both the fly TRPML and mammalian TRPML1 are optimally tuned to the lysosomal environment of the respective cells. Our data suggest that when expressed in human cells, the insect TRPML may be optimally activated in late-endosomes or other organelles that have slightly higher pH than lysosomes. It would be interesting to also know the pH dependence of TRPML2 and TRPML3. At least for $TRPML3^{Va}$, the constitutive whole-cell current was reported to be smaller at pH 4.6 than at pH 7.4, suggesting an inhibitory effect by strong acid (16). For wild type TRPML3 activated under Na^+-free conditions, acid was also shown to be only inhibitory (14). Therefore, TRPML displays similar pH dependence as mammalian TRPML1, but not TRPML3; however, its pH sensitivity is shifted to less acidic conditions than mammalian TRPML1.

Finally, like all mammalian TRPML channels, TRPML is activated by $PI(3,5)P_2$ and it displays an inwardly rectifying I-V relationship with very little outward current at positive potentials. These results are consistent with the findings *in vivo* suggesting that the vesicular trafficking defects observed in the *Drosophila trpml*^{1} mutants is remarkably similar to those observed in the *Drosophila fab1* mutants, which are unable to synthesize $PI(3,5)P_2$ (27, 40). The $PI(3,5)P_2$-elicited TRPML current is blocked by $PI(4,5)P_2$, which is consistent with mammalian TRPML1 (23). However, different from TRPML1, TRPML was not blocked by $PI(3,4)P_2$ or $PI(3,4,5)P_3$. Thus, although all TRPML channels are regulated by phosphoinositides, the selectivity among different phosphoinositide species is unique for each TRPML. It would be interesting to examine the phosphoinositde sensitivity of TRPML2 and TRPML3.

In conclusion, *Drosophila* TRPML forms $PI(3,5)P_2$-activated inwardly rectifying channels on both endolysosomal and plasma membrane when expressed in HEK293 cells. The channel is specifically inhibited by $PI(4,5)P_2$, but not other related phosphoinositides. Currents mediated by TRPML are cation non-selective, with excellent permeability to divalent cations, including Ca^{2+} and Fe^{2+}. The TRPML-mediated current is blocked by trivalent cations, Fe^{3+}, La^{3+}, and Gd^{3+}, and it is strongly potentiated by moderately low pH and inhibited by more acidic pH. Thus, our data suggest that TRPML resembles more closely to mammalian TRPML1 than TRPML2 or TRPML3. Supporting this conclusion, transgenic expression of human TRPML1 coding sequence in the fruit fly partially rescued the pupal lethality phenotype of the *trpml*^{1} mutation. The incomplete effect may be explained by the differences between *Drosophila* TRPML and mammalian TRPML1, such as differential pH dependence, plasma membrane localization, and/or sensitivity to $PI(3,4)P_2$, and $PI(3,4,5)P_3$. Collectively, these data support the notion that the *Drosophila* system serves an excellent model for assessing the functions of TRPML1 in cell physiology and provide molecular basis for understanding some of the differences between mammalian and insect TRPML channels in the regulation of lysosome membrane trafficking, endocytosis and autophagy.

Acknowledgments—We thank Drs. Paul Luzio and Haoxing Xu for cDNA constructs and Alemayehu A. Gorfe for critical data discussion.

REFERENCES

1. Cheng, X., Shen, D., Samie, M., and Xu, H. (2010) Mucolipins: Intracellular TRPML1–3 channels. *FEBS Letters* **584,** 2013–2021
2. Bargal, R., Avidan, N., Ben-Asher, E., Olender, Z., Zeigler, M., Frumkin, A., Raas-Rothschild, A., Glusman, G., Lancet, D., and Bach, G. (2000) Identification of the gene causing mucolipidosis type IV. *Nat. Genet.* **26,** 118–123
3. Bassi, M. T., Manzoni, M., Monti, E., Pizzo, M. T., Ballabio, A., and Borsani, G. (2000) Cloning of the gene encoding a novel integral membrane protein, mucolipidin-and identification of the two major founder mutations causing mucolipidosis type IV. *Am. J. Hum. Genet.* **67,** 1110–1120
4. Sun, M., Goldin, E., Stahl, S., Falardeau, J. L., Kennedy, J. C., Jr., Acierno, J. S., Jr., Bove, C., Kaneski, C. R., Nagle, J., Bromley, M. C., Colman, M., Schiffmann, R., and Slaugenhaupt, S. A. (2000) Mucolipidosis type IV is caused by mutations in a gene encoding a novel transient receptor potential channel. *Hum. Mol. Genet.* **9,** 2471–2478
5. Altarescu, G., Sun, M., Moore, D. F., Smith, J. A., Wiggs, E. A., Solomon, B. I., Patronas, N. J., Frei, K. P., Gupta, S., Kaneski, C. R., Quarrell, O. W., Slaugenhaupt, S. A., Goldin, E., and Schiffmann, R. (2002) The neurogenetics of mucolipidosis type IV. *Neurology* **59,** 306–313
6. Chen, C. S., Bach, G., and Pagano, R. E. (1998) Abnormal transport along the lysosomal pathway in Mucolipidosis, type IV disease. *Proc. Natl. Acad. Sci. U.S.A.* **95,** 6373–6378
7. Bach, G. (2005) Mucolipin 1: endocytosis and cation channel–a review. *Pflugers Archiv.* **451,** 313–317
8. Venugopal, B., Browning, M. F., Curcio-Morelli, C., Varro, A., Michaud, N., Nanthakumar, N., Walkley, S. U., Pickel, J., and Slaugenhaupt, S. A. (2007) Neurologic, gastric, and opthalmologic pathologies in a murine model of mucolipidosis type IV. *Am. J. Hum. Genet.* **81,** 1070–1083
9. Micsenyi, M. C., Dobrenis, K., Stephney, G., Pickel, J., Vanier, M. T., Slaugenhaupt, S. A., and Walkley, S. U. (2009) Neuropathology of the $Mcoln1^{-/-}$ knockout mouse model of mucolipidosis type IV. *J. Neuropathol. Exp. Neurol.* **68,** 125–135

10. Chandra, M., Zhou, H., Li, Q., Muallem, S., Hofmann, S. L., and Soyombo, A. A. (2011) A role for the Ca^{2+} channel TRPML1 in gastric acid secretion, based on analysis of knockout mice. *Gastroenterology* **140,** 857–867
11. Kim, H. J., Soyombo, A. A., Tjon-Kon-Sang, S., So, I., and Muallem, S. (2009) The Ca^{2+} channel TRPML3 regulates membrane trafficking and autophagy. *Traffic* **10,** 1157–1167
12. Grimm, C., Jörs, S., Guo, Z., Obukhov, A. G., and Heller, S. (2012) Constitutive activity of TRPML2 and TRPML3 channels versus activation by low extracellular sodium and small molecules. *J. Biol. Chem.* **287,** 22701–22708
13. Kim, H. J., Li, Q., Tjon-Kon-Sang, S., So, I., Kiselyov, K., and Muallem, S. (2007) Gain-of-function mutation in TRPML3 causes the mouse Varitint-Waddler phenotype. *J. Biol. Chem.* **282,** 36138–36142
14. Kim, H. J., Li, Q., Tjon-Kon-Sang, S., So, I., Kiselyov, K., Soyombo, A. A., and Muallem, S. (2008) A novel mode of TRPML3 regulation by extracytosolic pH absent in the varitint-waddler phenotype. *EMBO J.* **27,** 1197–1205
15. Lev, S., Zeevi, D. A., Frumkin, A., Offen-Glasner, V., Bach, G., and Minke, B. (2010) Constitutive activity of the human TRPML2 channel induces cell degeneration. *J. Biol. Chem.* **285,** 2771–2782
16. Xu, H., Delling, M., Li, L., Dong, X., and Clapham, D. E. (2007) Activating mutation in a mucolipin transient receptor potential channel leads to melanocyte loss in varitint-waddler mice. *Proc. Natl. Acad. Sci. U.S.A.* **104,** 18321–18326
17. Grimm, C., Cuajungco, M. P., van Aken, A. F., Schnee, M., Jörs, S., Kros, C. J., Ricci, A. J., and Heller, S. (2007) A helix-breaking mutation in TRPML3 leads to constitutive activity underlying deafness in the varitint-waddler mouse. *Proc. Natl. Acad. Sci. U.S.A.* **104,** 19583–19588
18. Nagata, K., Zheng, L., Madathany, T., Castiglioni, A. J., Bartles, J. R., and García-Añoveros, J. (2008) The varitint-waddler (Va) deafness mutation in TRPML3 generates constitutive, inward rectifying currents and causes cell degeneration. *Proc. Natl. Acad. Sci. U.S.A.* **105,** 353–358
19. Di Palma, F., Belyantseva, I. A., Kim, H. J., Vogt, T. F., Kachar, B., and Noben-Trauth, K. (2002) Mutations in Mcoln3 associated with deafness and pigmentation defects in varitint-waddler (Va) mice. *Proc. Natl. Acad. Sci. U.S.A.* **99,** 14994–14999
20. Dong, X. P., Wang, X., Shen, D., Chen, S., Liu, M., Wang, Y., Mills, E., Cheng, X., Delling, M., and Xu, H. (2009) Activating mutations of the TRPML1 channel revealed by proline-scanning mutagenesis. *J. Biol. Chem.* **284,** 32040–32052
21. Dong, X. P., Cheng, X., Mills, E., Delling, M., Wang, F., Kurz, T., and Xu, H. (2008) The type IV mucolipidosis-associated protein TRPML1 is an endolysosomal iron release channel. *Nature* **455,** 992–996
22. Dong, X. P., Shen, D., Wang, X., Dawson, T., Li, X., Zhang, Q., Cheng, X., Zhang, Y., Weisman, L. S., Delling, M., and Xu, H. (2010) $PI(3,5)P_2$ controls membrane trafficking by direct activation of mucolipin Ca^{2+} release channels in the endolysosome. *Nat. Commun.* **1,** 38
23. Zhang, X., Li, X., and Xu, H. (2012) Phosphoinositide isoforms determine compartment-specific ion channel activity. *Proc. Natl. Acad. Sci. U.S.A.* **109,** 11384–11389
24. Treusch, S., Knuth, S., Slaugenhaupt, S. A., Goldin, E., Grant, B. D., and Fares, H. (2004) *Caenorhabditis elegans* functional orthologue of human protein h-mucolipin-1 is required for lysosome biogenesis. *Proc. Natl. Acad. Sci. U.S.A.* **101,** 4483–4488
25. Sun, T., Wang, X., Lu, Q., Ren, H., and Zhang, H. (2011) CUP-5, the *C. elegans* ortholog of the mammalian lysosomal channel protein MLN1/TRPML1, is required for proteolytic degradation in autolysosomes. *Autophagy* **7,** 1308–1315
26. Venkatachalam, K., Long, A. A., Elsaesser, R., Nikolaeva, D., Broadie, K., and Montell, C. (2008) Motor deficit in a *Drosophila* model of mucolipidosis type IV due to defective clearance of apoptotic cells. *Cell* **135,** 838–851
27. Wong, C. O., Li, R., Montell, C., and Venkatachalam, K. (2012) *Drosophila* TRPML is required for TORC1 activation. *Curr. Biol.* **22,** 1616–1621
28. Venkatachalam, K., Wong, C. O., and Montell, C. (2013) Feast or famine: role of TRPML in preventing cellular amino acid starvation. *Autophagy* **9,** 98–100
29. Rohács, T., Chen, J., Prestwich, G. D., and Logothetis, D. E. (1999) Distinct specificities of inwardly rectifying K^+ channels for phosphoinositides. *J. Biol. Chem.* **274,** 36065–36072
30. Xiao, R., Tang, J., Wang, C., Colton, C. K., Tian, J., and Zhu, M. X. (2008) Calcium plays a central role in the sensitization of TRPV3 channel to repetitive stimulations. *J. Biol. Chem.* **283,** 6162–6174
31. Boussif, O., Lezoualc'h, F., Zanta, M. A., Mergny, M. D., Scherman, D., Demeneix, B., and Behr, J. P. A versatile vector for gene and oligonucleotide transfer into cells in culture and in vivo: polyethylenimine. (1995) A versatile vector for gene and oligonucleotide transfer into cells in culture and in vivo: polyethylenimine. *Proc. Natl. Acad. Sci. U.S.A.* **92,** 7297–7301
32. Thomas, M., and Klibanov, A. M. (2002) Enhancing polyethylenimine's delivery of plasmid DNA into mammalian cells. *Proc. Natl. Acad. Sci. U.S.A.* **99,** 14640–14645
33. Bischof, J., Maeda, R. K., Hediger, M., Karch, F., and Basler, K. (2007) An optimized transgenesis system for *Drosophila* using germ-line-specific phiC31 integrases. *Proc. Natl. Acad. Sci. U.S.A.* **104,** 3312–3317
34. Vaithianathan, T., Bukiya, A., Liu, J., Liu, P., Asuncion-Chin, M., Fan, Z., and Dopico, A. (2008) Direct regulation of BK channels by phosphatidylinositol 4,5-bisphosphate as a novel signaling pathway. *J. Gen. Physiol.* **132,** 13–28
35. Zhu, X., Jiang, M., and Birnbaumer, L. (1998) Receptor-activated Ca^{2+} influx via human Trp3 stably expressed in human embryonic kidney (HEK)293 cells. Evidence for a non-capacitative Ca^{2+} entry. *J. Biol. Chem.* **273,** 133–142
36. Shen, D., Wang, X., Li, X., Zhang, X., Yao, Z., Dibble, S., Dong, X. P., Yu, T., Lieberman, A. P., Showalter, H. D., and Xu, H. (2012) Lipid storage disorders block lysosomal trafficking by inhibiting a TRP channel and lysosomal calcium release. *Nat. Commun.* **3,** 731
37. Swetha, M. G, Sriram, V., Krishnan, K. S., Oorschot, V. M., ten Brink, C., Klumperman, J., and Mayor, S. (2011) Lysosomal membrane protein composition, acidic pH and sterol content are regulated via a light-dependent pathway in metazoan cells. *Traffic* **12,** 1037–1055
38. Mellman, I., Fuchs, R., and Helenius, A. (1986) Acidification of the endocytic and exocytic pathways. *Annu. Rev. Biochem.* **55,** 663–700
39. Cang, C., Zhou, Y., Navarro, B., Seo, Y. J., Aranda, K., Shi, L., Battaglia-Hsu, S., Nissim, I., Clapham, D. E., and Ren, D. (2013) mTOR regulates lysosomal ATP-sensitive two-pore Na^+ channels to adapt to metabolic state. *Cell* **152,** 778–790
40. Rusten, T. E., Rodahl, L. M., Pattni, K. , Englund, C., Samakovlis, C., Dove, S., Brech, A., and Stenmark, H. (2006) Fab1 phosphatidylinositol 3-phosphate 5-kinase controls trafficking but not silencing of endocytosed receptors. *Mol. Biol. Cell* **17,** 3989–4001